



## **Position-Specific Substitution in Cellulose Ethers Studied by DNP Enhanced Solid-State NMR Spectroscopy**

Downloaded from: <https://research.chalmers.se>, 2025-09-25 12:09 UTC

Citation for the original published paper (version of record):

Karlsson, H., Pinon, A., Karlson, L. et al (2025). Position-Specific Substitution in Cellulose Ethers Studied by DNP Enhanced Solid-State NMR


Spectroscopy. Magnetic Resonance in Chemistry, 63(8): 560-568. <http://dx.doi.org/10.1002/mrc.5535>

N.B. When citing this work, cite the original published paper.

## RESEARCH ARTICLE

## OPEN ACCESS

# Position-Specific Substitution in Cellulose Ethers Studied by DNP Enhanced Solid-State NMR Spectroscopy

Hampus Karlsson<sup>1,2,3</sup> | Arthur C. Pinon<sup>4</sup> | Leif Karlson<sup>2,5</sup> | Helena Wassenius<sup>2,5</sup> | Frida Iselau<sup>2,6,7</sup> | Staffan Schantz<sup>2,4,7</sup> | Lars Evenäs<sup>1,2,3</sup> 

<sup>1</sup>Department of Chemistry and Chemical Engineering, Chalmers University of Technology, Gothenburg, Sweden | <sup>2</sup>FibRe-Centre for Lignocellulose-Based Thermoplastics, Department of Chemistry and Chemical Engineering, Chalmers University of Technology, Gothenburg, Sweden | <sup>3</sup>Wallenberg Wood Science Center, Chalmers University of Technology, Gothenburg, Sweden | <sup>4</sup>Swedish NMR Centre, Department of Chemistry and Molecular Biology, University of Gothenburg, Gothenburg, Sweden | <sup>5</sup>Nouryon Functional Chemicals AB, Stenungsund, Sweden | <sup>6</sup>Technical Operations, Science and Innovation, Pharmaceutical Technology & Development, Operations, AstraZeneca, Gothenburg, Sweden | <sup>7</sup>Oral Product Development, Pharmaceutical Technology & Development, Operations, AstraZeneca, Gothenburg, Sweden

**Correspondence:** Lars Evenäs ([lars.evenas@chalmers.se](mailto:lars.evenas@chalmers.se))

**Received:** 5 March 2025 | **Revised:** 7 May 2025 | **Accepted:** 12 May 2025

**Funding:** This work was supported by FibRe Competence Centre, Wallenberg Wood Science Center.

**Keywords:** cellulose ethers | DNP | EHEC | MEHEC | solid-state NMR | substitution

## ABSTRACT

Ethyl hydroxyethyl cellulose (EHEC) and methyl ethyl hydroxyethyl cellulose (MEHEC) are hydrophilic cellulose ethers commonly employed as rheology modifiers in diverse industrial applications. The performance of these polymers, and their resistance to degradation by various cellulase enzymes, depends on their intricate molecular structure. Distribution of the etherifying groups, within the anhydroglucose units and along the polymer chain, is the key property to control. However, characterizing such structural properties is challenging, necessitating the development of novel analysis methods. In this study, we demonstrate the application of solid-state nuclear magnetic resonance (NMR) spectroscopy, enhanced by dynamic nuclear polarization (DNP), for this purpose. We prove that the hydrophilic EHEC and MEHEC samples are homogeneously swelled in D<sub>2</sub>O/H<sub>2</sub>O-based radical solutions, a necessity to ensure uniform DNP enhancement throughout the material. And we illustrate how the high sensitivity enhancements obtained can be used to perform selective, *J*-coupling-based C1 to C2 transfer experiments to measure the fraction of substituted C2 positions in these cellulose ethers. Moreover, with further refinement, the methodology outlined in this work holds promise for elucidating C3-specific substitution patterns.

## 1 | Introduction

Etherified cellulose materials can be found in many different industrial applications. By substituting the hydroxyl groups on the cellulose backbone into ether groups, functionally diverse materials can be created. Methyl cellulose (MC) and ethyl cellulose (EC) typically have applications in food and drug industry [1, 2]. Other derivatives with multiple different side chains such as methyl ethyl hydroxyethyl cellulose (MEHEC) and ethyl hydroxyethyl cellulose (EHEC) have for instance found use as rheology modifiers in areas such as the paint and construction

industry. The rheology modifying effect can be reduced if the cellulose ether is attacked by cellulase enzymes and the  $\beta$ -1,4-linkage between the anhydroglucose units (AGUs) is cleaved. This can happen if a paint is contaminated with cellulase-producing microorganisms, which may come from equipment and surroundings [3]. For such enzymatic attacks, the degree of substitution (DS) and the distribution of the etherifying side chains along the cellulose backbone will affect the accessibility for cleavage and thus also the biostability [4, 5]. DS refers to how many of the hydroxy groups on the AGU in the cellulose backbone that have reacted (on average along the polymer); it takes

This is an open access article under the terms of the [Creative Commons Attribution](https://creativecommons.org/licenses/by/4.0/) License, which permits use, distribution and reproduction in any medium, provided the original work is properly cited.

© 2025 The Author(s). *Magnetic Resonance in Chemistry* published by John Wiley & Sons Ltd.

on a numerical value between 0 and 3, where a DS = 3, indicates that all three hydroxy groups have been substituted [6]. The DS value is used for substituents, such as methyl and ethyl groups, that blocks the hydroxy groups from participating in further nucleophilic attacks. When the hydroxy groups on cellulose instead are reacted with a molecule (such as ethylene oxide [EO] for instance), that in turn generates a new nucleophilic moiety that can react again, the sidechains can in theory become infinitely long. For such substituents, one reports the molar substitution (MS), which is the number of moles of the substituent per AGU [7]. Because of the intricate relationship between DS/MS and properties of the final modified cellulose polymer, control of the substitution reactions and the possibility to measure DS and MS and side chain distribution becomes of outmost importance. Traditionally, these types of properties have been investigated with a variety of chemical, chromatographic and spectroscopic methods such as gas chromatography (GC), high-performance liquid chromatography (HPLC), size exclusion chromatography (SEC), mass spectrometry (MS) and nuclear magnetic resonance (NMR) spectroscopy [6, 8, 9]. However, these existing methods are all associated with drawbacks of their own. GC methods for analyzing hydroxyethyl-based side chains, might for instance include tedious acid-based degradation steps [10], liquid-state NMR is limited in what concentrations that are feasible to use, and ordinary  $^{13}\text{C}$ -detected room temperature solid-state NMR is slow due to the low abundance of  $^{13}\text{C}$ . Dynamic nuclear polarization (DNP), on the other hand, is an NMR technique used to enhance NMR signals and thus speed up NMR experiments. The DNP method is most often used within the solid-state NMR context, typically in combination with magic angle spinning (MAS) and forms an attractive option for studies of cellulose ethers.

DNP was initially explored in the 1950s and it has re-emerged as method in the recent decades as commercial DNP equipment have become more widely available [11]. During a DNP-enhanced solid-state NMR experiment, the NMR sample is irradiated with microwaves in the presence of unpaired electrons (i.e., radicals) at low temperatures (typically 100 K). This leads to a transfer of the high spin polarization of the unpaired electrons to the atomic nuclei of the sample and enhances their NMR signal by orders of magnitude [12–15]. Before the DNP-NMR experiment, radicals are added to the sample with a solution containing organic molecules with unpaired electrons; it is moreover required that the solution wets the polymer material. AMUPol [16] and TEKPol [17] are examples of well-established radicals for DNP usage. Cryoprotecting agents such as glycerol- $d_8$  [18] or DMSO- $d_6$  [19] might also be added to the solution; although radical solutions without cryoprotecting agents have been shown to give high DNP sensitivity enhancement in cellulose materials [20–22]. We do not add any cryoprotecting agent to the radical solutions in our study, as the sample material, EHEC and MEHEC readily swell in contact with water-based solutions. For cellulosic materials, it is also an option to evaporate the radical solvent in a desiccator to get the radical adsorbed on the surface of the solid [23].

DNP-enhanced solid-state NMR has been successfully deployed before to study cellulose ethers and cellulose-related materials [20, 23–29]. Especially, studies such as [20], focusing on the molecular regioselectivity of substitution in cellulose ethers, are important to contextualize our study. The study by [20] focuses on MC while our study focuses on EHEC and MEHEC, which

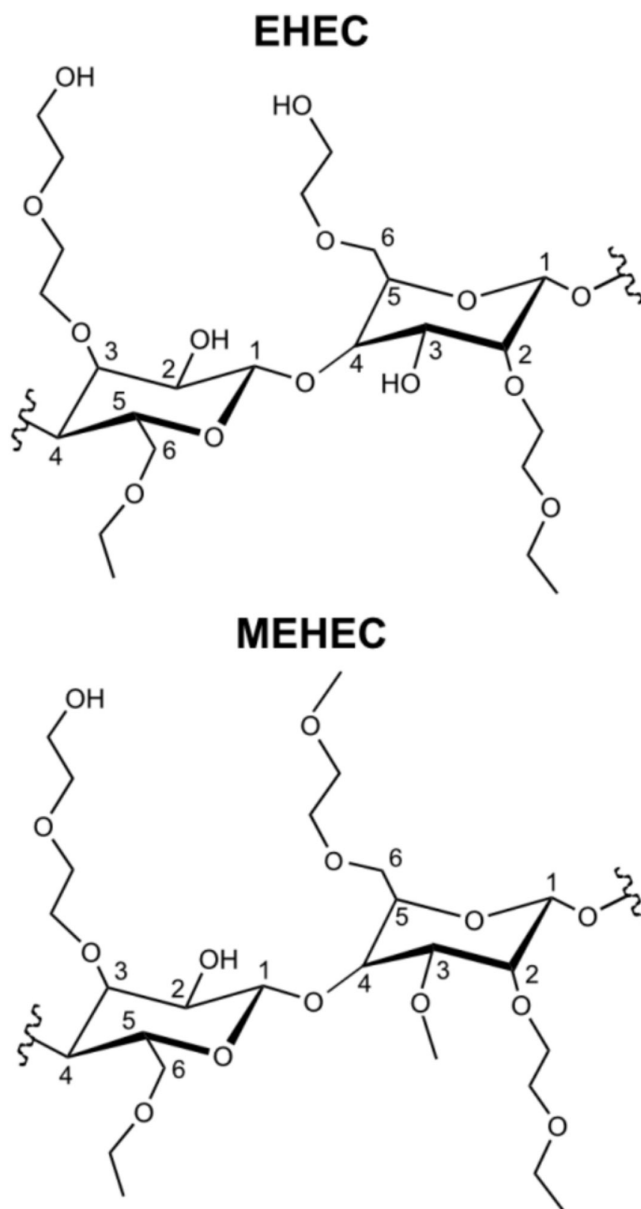


**FIGURE 1** | Molecular structures of possible repeating units of ethyl hydroxy ethyl cellulose (EHEC) and methyl ethyl hydroxy ethyl cellulose (MEHEC). In MEHEC, additional methyl groups are introduced, making molecular structure more complex.

are hydrophilic cellulose ethers with significantly more heterogeneous side chains (Figure 1) than MC, and in addition, with an industrial large-scale synthesis origin. Target in our study is the substitution at the C2 position of the AGUs, and we hypothesize that it is possible to use DNP enhanced solid-state NMR and selective, 1D,  $J$ -coupling-based correlation experiments for this site-specific quantification.

## 2 | Experimental

### 2.1 | Sample Material and Radical Solution

EHEC and MEHEC samples were provided by Nouryon (Stenungsund, Sweden). All samples were of industrial,

large-scale synthesis origin and with natural abundance levels of the  $^1\text{H}$  and  $^{13}\text{C}$  isotopes. Samples were classified as either biostable or non-biostable based on their production method and further verified by the reduction of viscosity of their water solutions in the presence of cellulase. These cellulase resistance assays were done by measuring the viscosity after 60 min of cellulase exposure. A 1 wt % polymer solution in 50-mL buffer (pH 5.5) was stirred at 425 rpm in a Rheomat 108 viscometer and kept at a temperature of 35°C in presence of 0.375 units of cellulase EC3.2.1.4 from *Aspergillus niger* (Sigma-Aldrich). The solutions were stirred for 60 min after which the viscosity was noted as a fraction of the starting viscosity. The obtained values were considered a quantitative measure of the biostability of the polymer, and from here on, these values are referred to as %S60 values in the text. MS of EO and DS of ethyl groups were determined by GC following the degradation of the products with HBr in glacial acetic acid [10]. Determination of DS for methyl groups was done with a slightly modified method, and the degradation was carried out with HI in glacial acetic acid instead of HBr. The given values, from here on referred to as  $\text{MS}_{\text{EO}}$ ,  $\text{DS}_{\text{me}}$ , and  $\text{DS}_{\text{et}}$  correspond to the average numbers of EO, methyl, and ethyl groups per sugar unit, respectively. Radical solutions for DNP NMR experiments consisted of 12-mM AMUPol (cortecnet.com) dissolved in  $\text{D}_2\text{O}:\text{H}_2\text{O}$  (9:1 by volume) using  $\text{D}_2\text{O}$  (99.8% D, ARMAR Isotopes) and MilliQ water (resistivity 18.2 M $\Omega$ -cm at 25°C).  $^{13}\text{C}$  labeled sodium formate (Sigma-Aldrich) was added during relaxation experiments to measure  $T_{\text{DNP}}$  (longitudinal buildup time of proton  $z$ -magnetization under DNP conditions) of the radical solution. Typically, some 20 mg of cellulose ether material was wetted or swelled in 40  $\mu\text{L}$  of the radical solution prior to packing into a 3.2-mm DNP NMR sapphire rotor with a PTFE plug and a VESPEL cap.

## 2.2 | DNP System

DNP NMR experiments were performed on a 400-MHz Bruker Ascend DNP magnet. The system was equipped with a 263-GHz gyrotron and a 3.2-mm LTMAS DNP probe. Experiments were performed with MAS rates ranging from 8 to 10 kHz; for all  $J$ -coupling-based experiments, MAS rates of 10 kHz were used. The temperature measured on the output gas from the LTMAS probe was  $\sim 104\text{ K}$  for experiments run with the microwaves on.

## 2.3 | NMR Experiments

2D refocused INADEQUATE experiments [30, 31] were acquired with 64 points in the indirect dimension and 1k points in the direct dimension and 512 scans. Four-millisecond long delays for  $J$ -evolution in the spin-echoes were used and the relaxation delay between scans was set to  $1.3 \times T_{\text{DNP}} \approx 4.3\text{ s}$ . 1D selective,  $J$ -coupling-based experiments were carried out in the following manner: After a nonselective cross-polarization (CP) [32] transfer, a selective flip-back pulse (1-ms Gaussian pulse with 10% truncation level) was applied on the C1 carbon to flip the magnetization back to  $+z$ . After the flip-back, a 2-ms long continuous wave (CW) irradiation on the  $^1\text{H}$  channel followed to relax away remaining transverse

$^{13}\text{C}$  coherences ( $z$ -filter). The  $^1\text{H}$  CW was matched with the MAS rate (rotational resonance) [33]. Thereafter, the same selective, truncated Gaussian pulse was applied on C1 to flip the magnetization down again, whereby a perfect-echo [34–36] for coherence transfer via  $J$ -coupling followed (see for instance Figure 4, further down). For the selective flip-down pulse after the  $z$ -filter, the phase was  $x, x, x, x, \bar{x}, \bar{x}, \bar{x}, \bar{x}$ ; for the perfect-echo, the pulse phases were  $x, -y$ , and  $x$  for the  $\pi$ ,  $\pi/2$ , and  $\pi$  pulse. The phase of the receiver was  $\bar{y}, \bar{y}, \bar{y}, y, y, y, y$ . Control experiments with the  $\pi/2$  pulse in the perfect-echo removed were performed to quantify artefact signals from the shaped pulses. After Fourier transform, phasing, and baseline correction, the spectra from these control experiments were subtracted from the actual transfer experiments and the resulting difference spectra were integrated over the C2 peak. Also, these experiments were performed with the relaxation delay between scans set to  $1.3 \times T_{\text{DNP}}$  and typically between 2 and 4k scans. Longitudinal  $^1\text{H}$  relaxation times were measured with standard  $^1\text{H}$  detected saturation recovery pulse sequence and with a pulse sequence with a CP transfer step at the end for  $^{13}\text{C}$  detection. All NMR data were processed with Topspin 4.1.1 and Python 3 scripts; the “NmrGlue” [37] python module was used during the processing of data from the 1D transfer experiment, in order to plot in detail and study the impact of baseline corrections and phasing. Relaxation data from saturation recovery experiments was fitted to the stretched exponential function [38].

## 2.4 | Electron Microscopy

Scanning electron microscopy (SEM) images of the cellulose ether samples were acquired on a Zeiss Ultra 55 FEG scanning electron microscope. Acceleration voltage was set to 3.0 kV and the working distance was 11 mm during imaging. The samples were coated with a 10-nm gold layer with a Leica ACE600 sputter coater machine.

## 3 | Results

### 3.1 | DNP Signal Enhancement in Hydrophilic Cellulose Ethers

The hydrophilic cellulose ethers EHEC and MEHEC showed high DNP sensitivity enhancements ( $\epsilon_{\text{DNP}}$ ) in  $\text{D}_2\text{O}:\text{H}_2\text{O}$ -based radical solutions. This is exemplified by the  $^{13}\text{C}$  CP/MAS spectra of sample “EHEC2” (Figure 2a), which is a biostable cellulose ether and that showed a  $\epsilon_{\text{DNP}} \approx 120$ , here reported as the ratio of the spectrum integrals acquired with microwaves on/off. We choose to report the sensitivity enhancement like this here, but it should be kept in mind that the signal in the microwave off spectrum, likely is significantly reduced (up to 60%) due to depolarization phenomena associated with the AMUPol usage [39]. Thus, our polarization gain in terms of Boltzmann distributions would be around a factor of 50 for our DNP experiments performed with the microwaves turned on.

This strong signal enhancement can be attributed to the fact that the EHEC and MEHEC samples readily swell in the  $\text{D}_2\text{O}:\text{H}_2\text{O}$ -based radical solutions used in the experiments. The size of the



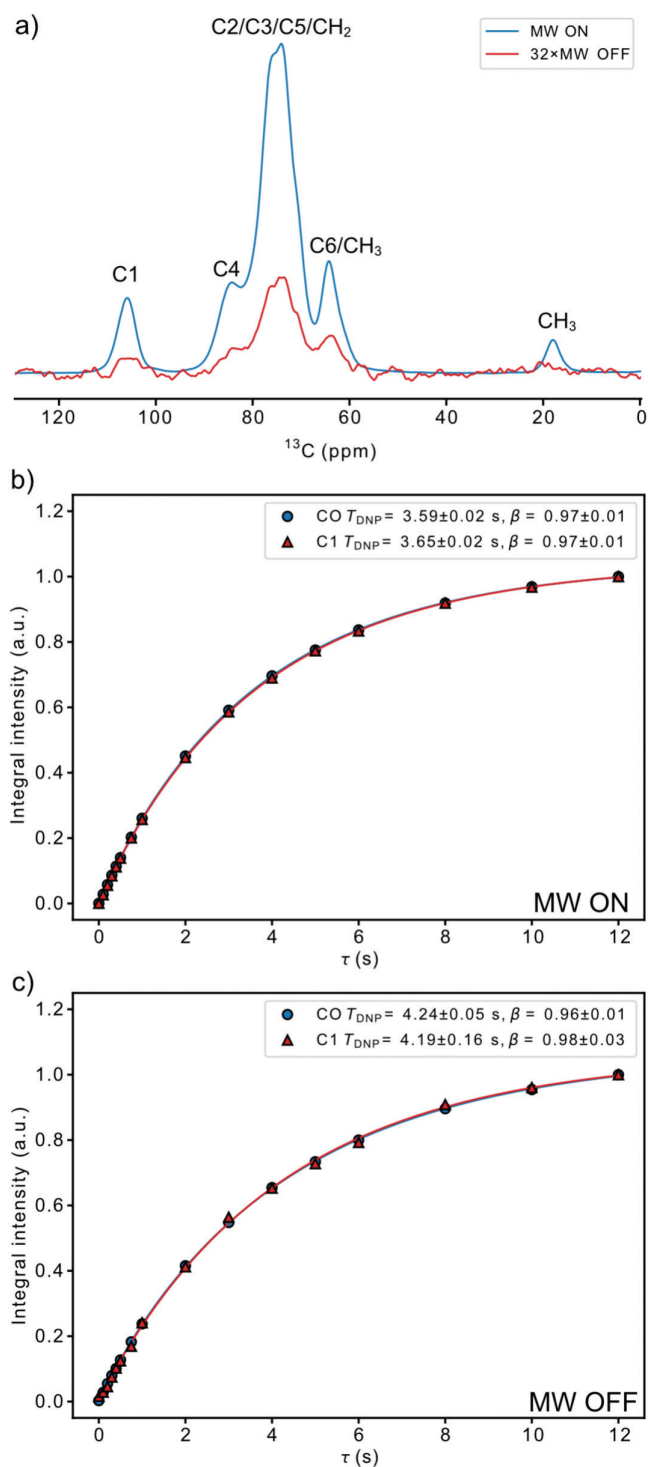


**FIGURE 2** | DNP enhanced  $^{13}\text{C}$  CP/MAS and  $^{13}\text{C}$  detected  $^1\text{H}$  saturation recovery data for the EHEC2 sample swelled in 12-mM AMUPol  $\text{D}_2\text{O}:\text{H}_2\text{O}$  (9:1) radical solution. (a)  $^{13}\text{C}$  CP/MAS spectra illustrating the large sensitivity enhancement when the microwaves are turned on/off. (b)  $^{13}\text{C}$  detected  $^1\text{H}$  saturation recovery data acquired with microwaves turned on, sodium formate was added to the radical solution, and the curves illustrate the practically identical buildup time detected on the carbonyl signal (CO) of the formate ion and the C1 carbon (C1) of EHEC. (c)  $^{13}\text{C}$  detected  $^1\text{H}$  saturation recovery data acquired with microwaves turned off, the buildup times differ from the ones observed with the microwaves turned on but are also here, practically the same for CO and C1.

industrially produced cellulose ether particles, when they are intact, is usually several tens of  $\mu\text{m}$  and aggregates thereof much larger (see Figure S1 for exemplifying SEM pictures of EHEC2). Such large particle size would lead to negligible DNP signal enhancements if the particles remained completely intact in the radical solution, as only the surface layer of the particles would become hyperpolarized. This size range  $\sim 20\text{--}100\mu\text{m}$  practically makes spin diffusion phenomena [40, 41] irrelevant for explaining the enhancements observed.  $^1\text{H}$  spin diffusion constants for our samples would be expected to be around  $10^{-15}\text{m}^2/\text{s}$  [42], this fact combined with that the  $^1\text{H}$   $T_1$  relaxation time of the dry EHEC2 powder at 100 K is  $13.3 \pm 1.7\text{s}$  (see Figure S2) and that most of our relaxation delays are less than 10 s means that  $^1\text{H}$  polarization never spin diffuses longer than  $\sim 0.1\mu\text{m}$ . Thus, swelling in the radical solution is likely the dominant factor determining enhancement. The question is though if swelling is homogeneous in the EHEC/MEHEC samples and if all parts are in good contact with the radical solution. This can be assessed by analyzing the saturation recovery data (Figure 1). The relaxation data acquired with the microwaves turned on (Figure 1b) show that the carbonyl signal of the sodium formate (i.e., known to be completely dissolved in the  $\text{D}_2\text{O}/\text{H}_2\text{O}$ -based radical solution) has the same  $T_{\text{DNP}}$  as the C1 signal of EHEC. This would be the case if the EHEC was homogeneously swelled, but it would also be the case if only a small fraction of the outermost layer of an EHEC-particle would be swelled. In such case, the enhanced signal from the swollen fraction of EHEC would dominate relaxation curve, and one would observe a  $T_{\text{DNP}}$  detected on the EHEC, very close to that observed on the formate in the radical solution, thus the fact that  $T_{\text{DNP}}$  is equal for CO and C1 in Figure 1b does not prove that EHEC is homogeneously swelled. However, in the relaxation data acquired with microwaves turned off (Figure 1c), the situation is different, then the swelled part is expected to relax fast due to paramagnetic relaxation enhancement effects from the radical [43–45], but it will not be enhanced (instead, slightly reduced due to depolarization). Thus, for the relaxation data acquired with the microwaves turned off (Figure 1c),  $T_{\text{DNP}}$  observed on C1 of EHEC will not approach that of CO in the radical solution unless the EHEC is fully, homogeneously swelled in the radical solution. We prove this by modelling the relaxation behavior of the EHEC system according to a biexponential model with different amounts of swelling (Supplementary discussion and Figure S3).

### 3.2 | Investigating C2 Substitution

The strong DNP sensitivity enhancements that we observed in these materials opened up the possibility of doing correlation experiments in a time-efficient manner. We were particularly interested in looking into the site-specific substitution on the AGU. It is well-known that both the DS and type of substituent affect the biostability of cellulose derivatives [5] and some studies [46] have indicated that, especially C2 and C3 substitution are more efficient in protecting against cellulose degradation. Because of this, methods that can inform on C2 substitution are valuable. The NMR chemical shift of the C2, C3, and C6 carbon of the AGU in cellulose is typically shifted 1–10 ppm downfield upon substitution [47]. This chemical shift change can be taken advantage of in order to estimate substitution. However,

in nonsubstituted cellulose both C2, C3, and C5 end up overlapping in the mid 70-ppm region [48]. In the heavily substituted EHEC and MEHEC systems, the chemical shift of C2 and C3 starts to vary due to substitution. Additional overlap is also introduced by the signals from the carbons in the CH<sub>2</sub> groups in the substituting side chains (ethyl and hydroxyethyl), and the highly amorphous character of these cellulose ethers due to the extensive substitution, further contributes to chemical shift

variations. Thus, there is a considerable overlap in the 70–90-ppm region in the CP/MAS spectra (such as Figure 1a) of these polymer systems. One way to get around the chemical shift overlapping problem of the 1D spectra is to use a 2D correlation experiment. The *J*-coupling-based, refocused INADEQUATE experiment [30, 31] is common, and several examples of its application to cellulosic materials under DNP-conditions exist [20, 22, 25, 29, 49]. Figure 3a shows a DNP enhanced, <sup>13</sup>C–<sup>13</sup>C

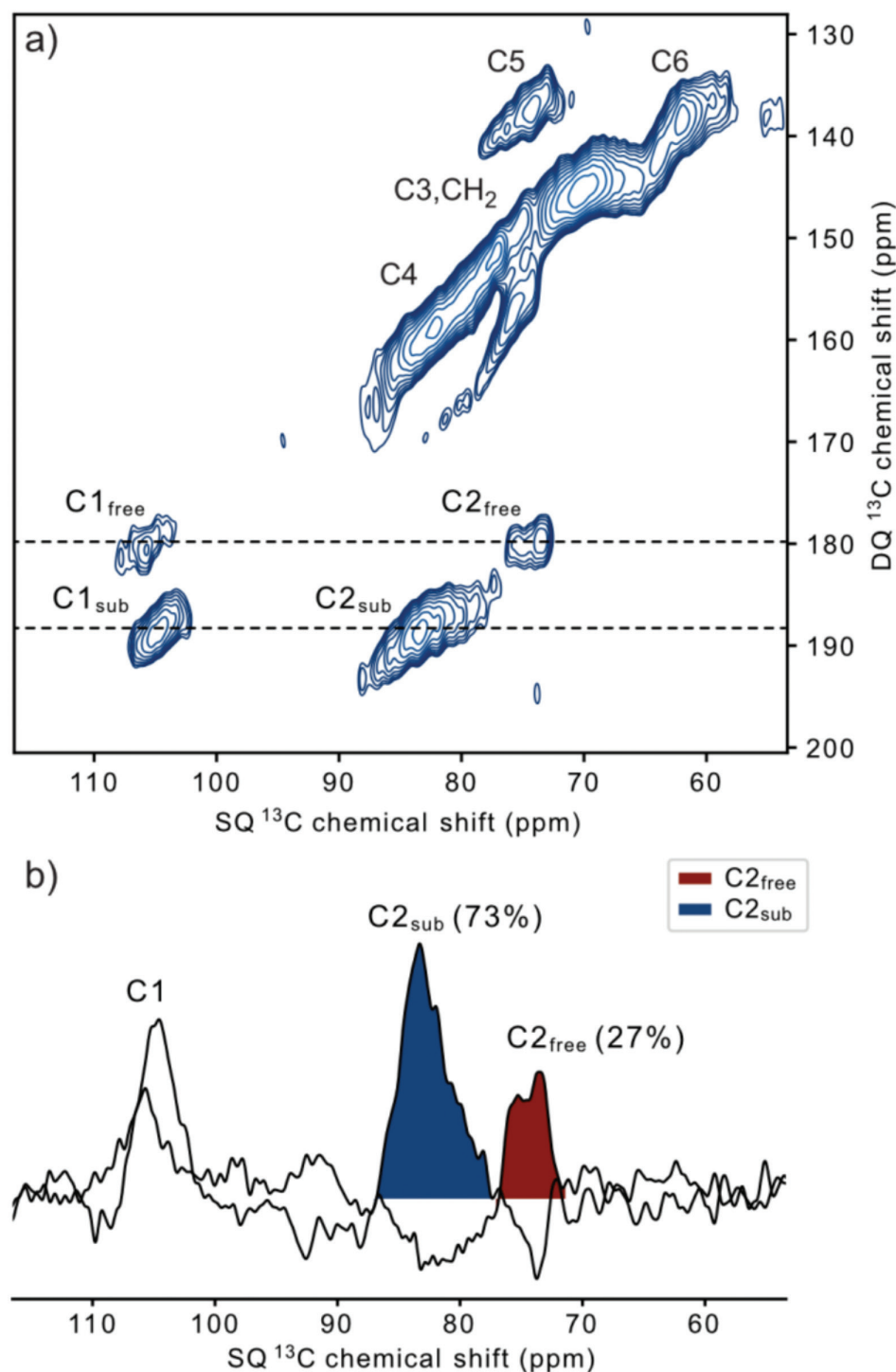


**FIGURE 3** | <sup>13</sup>C–<sup>13</sup>C DNP-enhanced refocused INADEQUATE spectrum of EHEC2. (a) 2D spectrum, it is easy to spot the C1/C2 correlations and chemical shift change of the substituted and free C2 positions, located around 75 and 84 ppm in the direct (horizontal) single quantum (SQ) dimension and around 180 and 189 ppm in the indirect (vertical) double quantum (DQ) dimension. (b) 1D slices of the rows in the 2D spectrum that correspond to the C1/C2 correlations, where peak integrals are indicative of substitution at the C2 position.

refocused INADEQUATE spectrum of EHEC2. It is clear in this 2D spectrum that there are two different correlations originating from the substituted and free C2 positions. Figure 3b exemplifies how for instance the 1D slices corresponding to these correlations can be analyzed to yield an estimate of the C2 specific substitution. Several factors will affect the accuracy of such quantifications but that will be addressed in the next Section 3.3.

Performing the DNP-enhanced,  $^{13}\text{C}$ - $^{13}\text{C}$  refocused INADEQUATE experiment on cellulose samples with natural abundance levels of  $^{13}\text{C}$  can be lengthy and take several days. The spectrum shown in Figure 3a was acquired in around 24 h, thanks to the high sensitivity enhancement ( $\epsilon_{\text{DNP}} \approx 120$ ). But since acquisition time for this type of experiment is lengthy and C2 substitution was our primary interest, we instead devised the selective 1D experiment illustrated in Figure 4. Using a selective 1D experiment saves time compared to a 2D experiment. The experiment outlined in Figure 4 (see details in Section 2) uses selective pulses and a z-filter for selecting C1, followed by transfer from C1 to C2. Initially, it was considered to use a selective CP transfer step to select C1, but it was soon realized that this is only feasible to do under fast MAS conditions [50]. Because of this, the strategy with a nonselective CP transfer, followed by the z-filter was chosen, a solution based on other examples from the solid-state NMR literature [42, 51]. However, the chosen z-filter approach is associated with both considerable signal losses during the shaped pulses and some artifact excitation (see Figure S4 for the properties of the selective pulses and the z-filter). The artefact excitation necessitated the control experiment in Figure 4b and the procedure of subtracting the control spectra (difference spectroscopy). After selection of the C1 signal, a perfect-echo was used for  $J$ -coupling mediated coherence transfer from C1 to C2. This choice was based on familiar examples from the solution state NMR literature [52, 53]. Usage of the perfect-echo means that the large signal from all non-coupled C1 nuclei will give signal in the spectrum as there is no means of coherence order filtering with the perfect-echo. The alternative would have been to use a pulse sequence fully analogous to the 2D refocused INADEQUATE experiment, i.e., with two  $\pi/2$  pulses between the spin-echoes (and no time evolution in the indirect dimension), create a double quantum coherence between them and then use a phase cycling scheme to select it. This was tested to some extent, but performance was poor on our cellulose samples under DNP-conditions (Figure S5). Another drawback of this approach would have been that the double quantum selective phase cycle only leads to transfer for half of the scans, which matters in the case of doing a 1D selective experiment, only starting with magnetization on C1. Because of the poor performance on our cellulose samples under DNP-conditions and the issue with transfer for only half of the scans, the simpler perfect-echo was chosen.

The experiment shown in Figure 4 was thus tested on a series of EHEC and MEHEC samples and the results of these experiments are summarized in Table 1, where also biostability data and DS/MS values of the substituents are shown. Ethers that were known to be biostable or non-biostable were included in the test sample set to see if the NMR method could discern any clear difference in C2 substitution between these two categories of ethers.

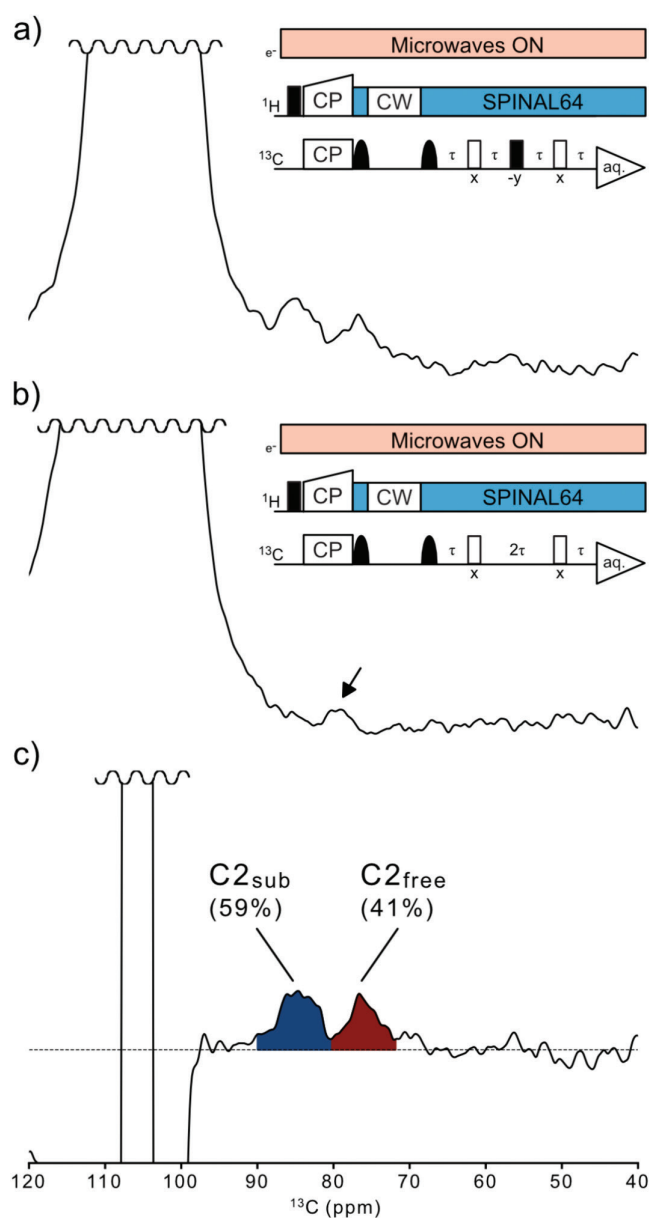


**FIGURE 4** | 1D,  $J$ -coupling-based correlation experiment for quantification of C2 substitution. (a) Spectrum from selective transfer experiment of the EHEC2 sample at MAS=10 kHz,  $T=104\text{ K}$ , and 12-mM AMUPol  $\text{D}_2\text{O}:\text{H}_2\text{O}$  (9:1) radical solution and 2048 scans/2h experimental time. The pulse sequence with selection step and perfect echo is shown. (b) Spectrum from the control experiment in which the  $\pi/2$  transfer pulse has been removed from the perfect echo. The spectrum thus only contains  $T_2$  decayed artifact signal indicated by the small black arrow. (c) Difference spectrum (transfer experiment (a)—control experiment (b)), here, the signals are assumed to come only from the  $J$ -coupling transfer and are thus integrated. The signal in spectral region 90.1–80.4 ppm is considered to originate from substituted C2 and the signal in the 80.4–71.9 ppm region from free, nonsubstituted C2. The percentage of the integral relative to the integral of the whole region is shown. A dashed line indicates the baseline.

The NMR spectra from the 1D correlation experiments underlying the results in Table 1 can be found in Figure S6. As can be seen in Table 1, the measured C2 substitution values do vary between the samples, but there is no clear difference in the C2

**TABLE 1** | Biostability, %S60, C2 site-specific substitution, and DS/MS values for the series of EHEC and MEHEC samples investigated. The second column shows if the ether is classified as biostable or not, based on production method. The third column shows %S60 (remaining viscosity after 60-min cellulase exposure). The fourth column shows measured C2 substitution from the 1D  $J$ -correlation experiments, errors represent one standard deviation and were estimated from sample EHEC1, the only sample with triplicate measurements. The three rightmost columns show the DS/MS for methyl, ethyl, and ethylene oxide groups obtained from gas chromatographic methods. Notice that also the EHEC samples contain some substituted  $\text{CH}_3$  groups, this is due to production technical factors.

Name	Classification	%S60 pH 5.5, 35°C	% C2 substituted (90.1–80.4 ppm)	DS <sub>me</sub>	DS <sub>et</sub>	MS <sub>EO</sub>
EHEC1	Non-biostable	63.7	53 ± 12	0.26	0.64	1.85
EHEC2	Biostable	75.8	59 ± 13	0.16	0.70	2.07
EHEC3	Biostable	81.4	54 ± 12	0.00	0.74	2.20
MEHEC1	Non-biostable	55.3	53 ± 12	0.30	0.42	1.52
MEHEC2	Biostable	81.7	63 ± 14	0.42	0.37	1.82

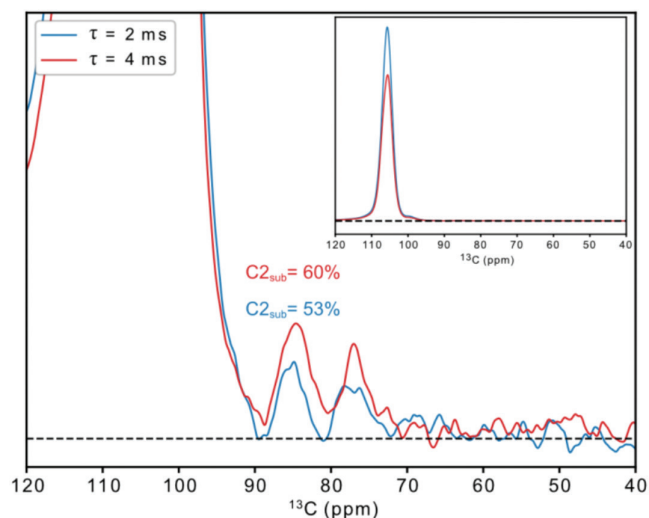


**FIGURE 5** | DNP-enhanced spectra from the 1D transfer experiment (no control spectra subtracted) acquired on the MEHEC2 sample with different  $\tau$  delay in the spin-echoes, showing a clear buildup of signal for the 4-ms delay. The buildup of signal and small difference in proportion of the  $\text{C2}_{\text{sub}}$  correlation signal supports the claim that differences in  $J_{\text{C1C2}}$  and  $T'_2$  are not a major problem affecting the results. The inner panel shows a zoomed-out view of the spectra, illustrating the  $T'_2$  decay of the large C1 signal.

substitution between the biostable and non-biostable ethers. Between the two MEHEC samples, there is an indication of a difference, but this is a too limited number of samples to draw any certain conclusions from. Yet, the method shown in Figure 4 offers a less time-consuming way than the 2D INADEQUATE experiment for obtaining semi-quantitative values of the C2 substitution. The three rightmost columns of Table 1 provide the DS/MS values for the substituents determined by chemical, non-NMR methods. These data are included as complementary information and to highlight the complexity of these polymers and illustrate that despite differences in substitution properties, the polymers can have similar biostability performance. Our method provides partial information about these polymers, it can tell about C2 substitution in a reasonably time efficient and accurate manner, but it cannot inform on what substituent there is on C2. To fully elucidate this and all the factors affecting substitution and biostability, it is likely that data from

complementary methods are necessary. Bos et al. [54] presented an LC–MS-based method developed on a related set of cellulose ethers. Such methods can provide information on the distribution of side chain lengths and may complement data from NMR methods such as the one outlined in Figure 4.

### 3.3 | Accuracy of the C2 Substitution Values

In the previous section, we suggest the usage of the selective 1D  $J$ -coupling-based experiment (Figure 4) to obtain correlation signals of the C2 carbons of the AGU, signals that can be integrated to get a measure of the fraction of substituted C2 positions. Despite the beneficial sensitivity enhancement properties of these hydrophilic cellulose ethers in  $\text{D}_2\text{O}/\text{H}_2\text{O}$  based radical solutions, the signal-to-noise ratios associated with these types of experiments are in general very low. These low signal-to-noise ratios make the obtained values for C2 substitution semi-quantitative in nature. Even so, the data we present here (Table 1, Figures S6 and S7) are acquired on industrially produced cellulose ethers with complex side-chains and no degradation steps or similar are included in the sample preparation step; thus, the DNP-enhanced solid-state NMR method allows the study of the samples intact and with technically no limit in degree of polymerization. In addition to a low signal-to-noise ratio, we have performed these experiments as difference spectroscopy, subtracting the spectra from the control experiments from the actual transfer experiments. This was done because of the aforementioned artefact signals that originate from the shaped pulses used in the z-filter (Figure S4). This process, the phasing, baseline correction, and subtraction of the spectra, is a very sensitive procedure to perform at these low signal-to-noise ratios and unavoidably opens up for some subjectivity. To obtain the numbers presented in Table 1, typically, the regions between the large C1 signals and their first sidebands were used to perform a fifth-order polynomial baseline correction of the transfer and control spectra (Figure S8), after this baseline correction, the spectra from the control experiments were subtracted. Potential differences in  $J_{\text{C1C2}}$  and  $T'_2$  between substituted and free C2 may also impact the magnitude of the correlation peak integrals and the resulting C2 substitution values. However, Figure 5 illustrates the buildup of peak intensity in the 1D transfer experiment for two different  $\tau$  delays for the MEHEC2 sample. We interpret the small difference in peak integral proportions as an indication



that differences in  $J_{\text{C1C2}}$  and  $T'_2$  are not a major problem affecting the results. Thus, we claim that if the 1D correlation experiments are done carefully and with good control of potential artefact signals, processing and peak integration, reliable semi-quantitative values of C2 substitution can be obtained.

## 4 | Conclusion

In this work, we have shown how a selective 1D,  $J$ -coupling-based correlation experiment can be used to quantify the C2 substitution in hydrophilic cellulose ethers under DNP MAS conditions. The results from the selected set of cellulose ethers investigated exemplify how such an experiment could contribute to obtain information about substitution and biostability of cellulose ethers. We also believe that with some further development, and in combination with higher availability of DNP equipment with faster MAS rates combined with DNP enhancement, it could most possibly be attainable to deconvolute the C2 correlation signals and make indirect conclusions about substitution on C3. Under such conditions the experiment could be used to quantify substitution on both C2 and C3 in intact, industrially relevant cellulose ethers in one single experiment.

## Acknowledgments

The authors are grateful to the FibRe Competence Centre and the Wallenberg Wood Science Center for funding this research. We would also like to thank Anders Mårtensson for helping with acquiring SEM pictures of the cellulose ether samples. NMR experiments have been carried out at the Swedish NMR Centre in Gothenburg.

## Data Availability Statement

NMR data is available on zenodo: <https://doi.org/10.5281/zenodo.14269731>.

## References

1. H. C. Arca, L. I. Mosquera-Giraldo, V. Bi, D. Xu, L. S. Taylor, and K. J. Edgar, "Pharmaceutical Applications of Cellulose Ethers and Cellulose Ether Esters," *Biomacromolecules* 19 (2018): 2351–2376.
2. P. Nasatto, F. Pignon, J. Silveira, M. Duarte, M. Nosedá, and M. Rinaudo, "Methylcellulose, a Cellulose Derivative With Original Physical Properties and Extended Applications," *Polymers* 7 (2015): 777–803.
3. S. Cheroni, B. Gatti, G. Margheritis, C. Formantici, L. Perrone, and Y. M. Galante, "Enzyme Resistance and Biostability of Hydroxyalkylated Cellulose and Galactomannan as Thickeners in Waterborne Paints," *International Biodeterioration & Biodegradation* 69 (2012): 106–112.
4. I. E. Tothill and K. J. Seal, "Biodeterioration of Waterborne Paint Cellulose Thickeners," *International Biodeterioration & Biodegradation* 31 (1993): 241–254.
5. N. B. Erdal and M. Hakkarainen, "Degradation of Cellulose Derivatives in Laboratory, Man-Made, and Natural Environments," *Biomacromolecules* 23 (2022): 2713–2729.
6. S. Richardson and L. Gorton, "Characterisation of the Substituent Distribution in Starch and Cellulose Derivatives," *Analytica Chimica Acta* 497 (2003): 27–65.
7. M. W. Rutenberg and D. Solarek, "Starch Derivatives: Production and Uses," in *Starch Chemistry and Technology*, eds. R. L. Whistler, J. N. BeMiller, and E. F. Paschall (Academic Press, 1984): 313.
8. P. Mischnick and D. Momcilovic, *Advances in Carbohydrate Chemistry and Biochemistry* (Elsevier, 2010): 117–210.
9. Z. Zheng, Y. Su, and K. Schmidt-Rohr, "Corrected Solid-State  $^{13}\text{C}$  Nuclear Magnetic Resonance Peak Assignment and Side-Group Quantification of Hydroxypropyl Methylcellulose Acetyl Succinate Pharmaceutical Excipients," *Magnetic Resonance in Chemistry* 61 (2023): 595–605.
10. J. B. Stead and A. H. Hindley, "A Modified Method for the Analysis of Oxyethylene/Oxypropylene Copolymers by Chemical Fission and Gas Chromatography," *Journal of Chromatography A* 42 (1969): 470–475.
11. C. P. Slichter, "The Discovery and Renaissance of Dynamic Nuclear Polarization," *Reports on Progress in Physics* 77 (2014): 072501.
12. T. Maly, G. T. Debelouchina, V. S. Bajaj, et al., "Dynamic Nuclear Polarization at High Magnetic Fields," *Journal of Chemical Physics* 128, no. 5 (2008): 052211, <https://doi.org/10.1063/1.2833582>.
13. Q. Z. Ni, E. Daviso, T. V. Can, et al., "High Frequency Dynamic Nuclear Polarization," *Accounts of Chemical Research* 46 (2013): 1933–1941.
14. A. S. L. Thankamony, J. J. Wittmann, M. Kaushik, and B. Corzilius, "Dynamic Nuclear Polarization for Sensitivity Enhancement in Modern Solid-State NMR," *Progress in Nuclear Magnetic Resonance Spectroscopy* 102–103 (2017): 120–195.
15. B. Corzilius, "High-Field Dynamic Nuclear Polarization," *Annual Review of Physical Chemistry* 71 (2020): 143–170.
16. C. Sauvée, M. Rosay, G. Casano, et al., "Highly Efficient, Water-Soluble Polarizing Agents for Dynamic Nuclear Polarization at High Frequency," *Angewandte Chemie, International Edition* 52 (2013): 10858–10861.
17. A. Zagdoun, G. Casano, O. Ouari, et al., "Large Molecular Weight Nitroxide Biradicals Providing Efficient Dynamic Nuclear Polarization at Temperatures Up to 200 K," *Journal of the American Chemical Society* 135 (2013): 12790–12797.
18. G. Casano, H. Karoui, and O. Ouari, "Polarizing Agents: Evolution and Outlook in Free Radical Development for DNP," in *Handbook of High Field Dynamic Nuclear Polarization*, eds. B. Corzilius, R. G. Griffin, S. Vega, and V. K. Michaelis (John Wiley & Sons Ltd, 2020): 127–145.
19. V. K. Michaelis, T.-C. Ong, M. K. Kiesewetter, et al., "Topical Developments in High-Field Dynamic Nuclear Polarization," *Israel Journal of Chemistry* 54 (2014): 207–221.
20. P. Berruyer, M. Gericke, P. Moutzouri, et al., "Advanced Characterization of Regioselectively Substituted Methylcellulose Model Compounds by DNP Enhanced Solid-State NMR Spectroscopy," *Carbohydrate Polymers* 262 (2021): 117944.
21. A. Kumar, H. Durand, E. Zeno, et al., "The Surface Chemistry of a Nanocellulose Drug Carrier Unravelling by MAS-DNP," *Chemical Science* 11 (2020): 3868–3877.
22. J. Viger-Gravel, W. Lan, A. C. Pinon, et al., "Topology of Pretreated Wood Fibers Using Dynamic Nuclear Polarization," *Journal of Physical Chemistry C* 123 (2019): 30407–30415.
23. H. Takahashi, D. Lee, L. Dubois, M. Bardet, S. Hediger, and G. De Paëpe, "Rapid Natural-Abundance  $2\text{D }^{13}\text{C}$ – $^{13}\text{C}$  Correlation Spectroscopy Using Dynamic Nuclear Polarization Enhanced Solid-State NMR and Matrix-Free Sample Preparation," *Angewandte Chemie, International Edition* 51 (2012): 11766–11769.
24. P. Berruyer, P. Moutzouri, M. Gericke, et al., "Spatial Distribution of Functional Groups in Cellulose Ethers by DNP-Enhanced Solid-State NMR Spectroscopy," *Macromolecules* 55, no. 7 (2022): 2952–2958.
25. F. Deligey, M. A. Frank, S. H. Cho, et al., "Structure of In Vitro-Synthesized Cellulose Fibrils Viewed by Cryo-Electron Tomography and  $^{13}\text{C}$  Natural-Abundance Dynamic Nuclear Polarization Solid-State NMR," *Biomacromolecules* 23 (2022): 2290–2301.

26. A. Kirui, Z. Ling, X. Kang, et al., "Atomic Resolution of Cotton Cellulose Structure Enabled by Dynamic Nuclear Polarization Solid-State NMR," *Cellulose* 26 (2019): 329–339.
27. T. Kobayashi, I. I. Slowing, and M. Pruski, "Measuring Long-Range  $^{13}\text{C}$ – $^{13}\text{C}$  Correlations on a Surface Under Natural Abundance Using Dynamic Nuclear Polarization-Enhanced Solid-State Nuclear Magnetic Resonance," *Journal of Physical Chemistry C* 121 (2017): 24687–24691.
28. F. A. Perras, H. Luo, X. Zhang, N. S. Mosier, M. Pruski, and M. M. Abu-Omar, "Atomic-Level Structure Characterization of Biomass Pre- and Post-Lignin Treatment by Dynamic Nuclear Polarization-Enhanced Solid-State NMR," *Journal of Physical Chemistry. A* 121 (2017): 623–630.
29. W. Zhao, A. Kirui, F. Deligey, et al., "Solid-State NMR of Unlabeled Plant Cell Walls: High-Resolution Structural Analysis Without Isotopic Enrichment," *Biotechnology for Biofuels* 14 (2021): 14.
30. A. Lesage, M. Bardet, and L. Emsley, "Through-Bond Carbon–Carbon Connectivities in Disordered Solids by NMR," *Journal of the American Chemical Society* 121 (1999): 10987–10993.
31. S. Cadars, J. Sein, L. Duma, et al., "The Refocused INADEQUATE MAS NMR Experiment in Multiple Spin-Systems: Interpreting Observed Correlation Peaks and Optimising Lineshapes," *Journal of Magnetic Resonance* 188 (2007): 24–34.
32. A. Pines, M. G. Gibby, and J. S. Waugh, "Proton-Enhanced Nuclear Induction Spectroscopy. A Method for High Resolution NMR of Dilute Spins in Solids," *Journal of Chemical Physics* 56 (1972): 1776–1777.
33. T. G. Oas, R. G. Griffin, and M. H. Levitt, "Rotary Resonance Recoupling of Dipolar Interactions in Solid-State Nuclear Magnetic Resonance Spectroscopy," *Journal of Chemical Physics* 89 (1988): 692–695.
34. P. C. M. Van Zijl, C. T. W. Moonen, and M. Von Kienlin, "Homonuclear J Refocusing in Echo Spectroscopy," *Journal of Magnetic Resonance* (1969) 89, no. 1 (1990): 28–40, [https://doi.org/10.1016/0022-2364\(90\)90159-7](https://doi.org/10.1016/0022-2364(90)90159-7).
35. K. Takegoshi, K. Ogura, and K. Hikichi, "A Perfect Spin Echo in a Weakly Homonuclear J-Coupled Two Spin-System," *Journal of Magnetic Resonance* (1969) 84, no. 3 (1989): 611–615, [https://doi.org/10.1016/0022-2364\(89\)90127-3](https://doi.org/10.1016/0022-2364(89)90127-3).
36. T. Parella, "Towards Perfect NMR: Spin-Echo Versus Perfect-Echo Building Blocks," *Magnetic Resonance in Chemistry* 57 (2019): 13–29.
37. J. J. Helmus and C. P. Jaroniec, "Nmrglue: An Open Source Python Package for the Analysis of Multidimensional NMR Data," *Journal of Biomolecular NMR* 55 (2013): 355–367.
38. A. Narayanan, J. S. Hartman, and A. D. Bain, "Characterizing Non-exponential Spin-Lattice Relaxation in Solid-State NMR by Fitting to the Stretched Exponential" *Journal of Magnetic Resonance, Series A* 112 (1995): 56–58.
39. F. Mentink-Vigier, S. Paul, D. Lee, et al., "Nuclear Depolarization and Absolute Sensitivity in Magic-Angle Spinning Cross Effect Dynamic Nuclear Polarization," *Physical Chemistry Chemical Physics* 17 (2015): 21824–21836.
40. G. R. Khutsishvili, "Spin Diffusion," *Soviet Physics Uspekhi* 8 (1966): 743–769.
41. C. Ramanathan, "Dynamic Nuclear Polarization and Spin Diffusion in Nonconducting Solids," *Applied Magnetic Resonance* 34 (2008): 409–421.
42. J. Schlagnitweit, M. Tang, M. Baías, S. Richardson, S. Schantz, and L. Emsley, "A Solid-State NMR Method to Determine Domain Sizes in Multi-Component Polymer Formulations," *Journal of Magnetic Resonance* 261 (2015): 43–48.
43. A. J. Pell, G. Pintacuda, and C. P. Grey, "Paramagnetic NMR in Solution and the Solid State," *Progress in Nuclear Magnetic Resonance Spectroscopy* 111 (2019): 1–271.
44. B. Corzilius, L. B. Andreas, A. A. Smith, Q. Z. Ni, and R. G. Griffin, "Paramagnet Induced Signal Quenching in MAS–DNP Experiments in Frozen Homogeneous Solutions," *Journal of Magnetic Resonance* 240 (2014): 113–123.
45. S. Lange, A. H. Linden, Ü. Akbey, et al., "The Effect of Biradical Concentration on the Performance of DNP-MAS-NMR," *Journal of Magnetic Resonance* 216 (2012): 209–212.
46. M. Nojiri and T. Kondo, "Application of Regioselectively Substituted Methylcelluloses to Characterize the Reaction Mechanism of Cellulase," *Macromolecules* 29 (1996): 2392–2395.
47. I. Nehls, W. Wagenknecht, B. Philipp, and D. Stscherbina, "Characterization of Cellulose and Cellulose Derivatives in Solution by High Resolution  $^{13}\text{C}$ -NMR Spectroscopy," *Progress in Polymer Science* 19 (1994): 29–78.
48. A. Idström, S. Schantz, J. Sundberg, B. F. Chmelka, P. Gatenholm, and L. Nordstierna, " $^{13}\text{C}$  NMR Assignments of Regenerated Cellulose From Solid-State 2D NMR Spectroscopy," *Carbohydrate Polymers* 151 (2016): 480–487.
49. A. J. Rossini, A. Zagdoun, F. Hegner, et al., "Dynamic Nuclear Polarization NMR Spectroscopy of Microcrystalline Solids," *Journal of the American Chemical Society* 134 (2012): 16899–16908.
50. S. Laage, A. Marchetti, J. Sein, et al., "Band-Selective  $^1\text{H}$ – $^{13}\text{C}$  Cross-Polarization in Fast Magic Angle Spinning Solid-State NMR Spectroscopy," *Journal of the American Chemical Society* 130, no. 51 (2008): 17216–17217, <https://doi.org/10.1021/ja805926d>.
51. D. H. Zhou, K. D. Kloepper, K. A. Winter, and C. M. Rienstra, "Band-Selective  $^{13}\text{C}$  Homonuclear 3D Spectroscopy for Solid Proteins at High Field With Rotor-Synchronized Soft Pulses," *Journal of Biomolecular NMR* 34 (2006): 245–257.
52. J. Schlagnitweit, E. Steiner, H. Karlsson, and K. Petzold, "Efficient Detection of Structure and Dynamics in Unlabeled RNAs: The SELOPE Approach," *Chemistry—A European Journal* 24 (2018): 6067–6070.
53. M. R. M. Koos, G. Kummerlöwe, L. Kaltschnee, C. M. Thiele, and B. Luy, "CLIP-COSY: A Clean In-Phase Experiment for the Rapid Acquisition of COSY-Type Correlations," *Angewandte Chemie, International Edition* 55 (2016): 7655–7659.
54. T. S. Bos, J. S. Desport, A. Buijtenhuijs, et al., "Composition Mapping of Highly Substituted Cellulose-Ether Monomers by Liquid Chromatography–Mass Spectrometry and Probability-Based Data Deconvolution," *Journal of Chromatography A* 1689 (2023): 463758.

## Supporting Information

Additional supporting information can be found online in the Supporting Information section.